Electron energy loss in composite systems

J. M. Pitarke

Materia Kondentsatuaren Fisika Saila, Zientzi Falkultatea, Euskal Herriko Unibertsitatea, 644 Posta kutxatila, 48080 Bilbo,
Basque Country, Spain

J. B. Pendry

Condensed Matter Theory Group, The Blackett Laboratory, Imperial College, London SW7 2BZ, United Kingdom

P. M. Echenique

Materialen Fisika Saila, Kimika Falkultatea, Euskal Herriko Unibertsitatea, 1072 Posta kutxatila, 20080 Donostia,
Basque Country, Spain

The interaction of scanning transmission electron microscopy electrons with composite systems is investigated by following a mean-field theory of the effective response function. Expressions for the inverse longitudinal dielectric function of isolated spheres and cylinders are derived. Experimental valence loss spectra from SiO_2 polymorphs are analyzed and the insensitivity of the plasmon peak to the density of the material is explained. [S0163-1829(97)02715-X]

I. INTRODUCTION

Theoretical descriptions of the interaction of high-energy electron beams with surfaces and with small particles have been of basic importance in the development of scanning transmission electron microscopy. In the case of electrons moving on a definite trajectory energy-loss spectra have been calculated for planar interfaces,[1] spheres,[2] cylinders,[3–5] and more complex geometries.[6–8] On the other hand, electron-loss spectra for a broad beam geometry can be analyzed, via the concept of an effective medium, from the effective inverse longitudinal dielectric response. Effective-medium theories have been used for many years to analyze optical spectra and have also been proved to be useful to interpret electron-energy-loss experiments.

The $q=0$ limit of the average dielectric function for a system of spherical particles was first derived by Maxwell-Garnett,[9] within a mean-field approximation valid for small values of the volume occupied by the spheres. The Maxwell-Garnett dielectric function is successful in the optical range; however, in electron-energy-loss spectroscopy the electrons may excite modes with wavelengths smaller than the particle size and an appropriate dielectric function should retain information about the structure of the medium through a dependence on momentum transfer.

A momentum-dependent effective longitudinal dielectric function can be derived by equating the energy-loss probability of electrons passing through a composite system with the bulk-energy-loss probability. Fujimoto and Komaki[10] included all multipoles to derive, within the hydrodynamic approximation for a free-electron gas, the energy loss of a broad beam of fast electrons incident on an isolated sphere. This result for the energy loss was later generalized to obtain an expression that is valid for any local dielectric function inside the sphere.[11,12] Finally, these results have been recently extended and an expression for the effective longitudinal dielectric function of a random system of identical

spherical particles has been derived, within a mean-field approximation, by Barrera and Fuchs.[13] Maxwell-Garnett's theory[9] and previous theories for isolated spheres[11,12] represent the long-wavelength limit and the dilute limit, respectively, of the theory of Barrera and Fuchs. General expressions for the momentum-dependent effective inverse longitudinal dielectric function of a system of cylindrical particles, of interest in the investigation of valence loss spectra from zeolites[14] and tubular fullerenes,[15] are not available.

In this paper we present an alternative approach for the evaluation of the effective longitudinal response function of single isolated particles in an infinite medium. First of all, we reproduce former results for isolated spheres. Then we derive a general expression for the effective inverse longitudinal response function of isolated cylinders. Finally, we apply our theory to explain the experimental valence loss spectra obtained by McComb and Howie[14] from SiO_2 polymorphs, by modeling different silica polymorphs as less dense versions of the most dense material, stishovite.

II. THEORY

Suppose that a test charge density

$$\rho^{\text{ext}}(\mathbf{r},t) = \rho_0 e^{i(\mathbf{q}\cdot\mathbf{r}-\omega t)} \tag{2.1}$$

is introduced into an inhomogeneous medium of dielectric function $\epsilon(\mathbf{q},\mathbf{q}',\omega)$. It induces a charge $\rho^{\text{ind}}(\mathbf{r},t)$ in the system whose density Fourier components have the form[16]

$$\rho^{\text{ind}}(\mathbf{q}',\omega) = \rho_0 K(\mathbf{q}',\mathbf{q},\omega), \tag{2.2}$$

where $K(\mathbf{q}',\mathbf{q},\omega)$ represents the density-density response function of the medium

$$K(\mathbf{q},\mathbf{q}',\omega) = [\epsilon(\mathbf{q},\mathbf{q}',\omega)]^{-1} - \delta_{\mathbf{q},\mathbf{q}'}. \tag{2.3}$$

On the other hand, the probability per unit time for a swift electron to transfer momentum $\mathbf{q}$ and energy $\hbar\omega$ to an inho-

mogeneous electronic system is, within the first Born approximation, proportional to the dynamic structure factor[17]

$$S(\mathbf{q},\omega) = -\frac{4\pi^2 e^2}{\hbar q^2} \text{Im} \epsilon^{-1}(\mathbf{q},\mathbf{q},\omega). \tag{2.4}$$

Thus, in order to interpret electron-energy-loss experiments, we are interested in the evaluation of the momentum dependent effective inverse longitudinal dielectric function

$$\epsilon_{\text{eff}}^{-1}(\mathbf{q},\omega) = \epsilon^{-1}(\mathbf{q},\mathbf{q},\omega), \tag{2.5}$$

which can be derived after projecting the induced charged density $\rho^{\text{ind}}(\mathbf{r},t)$ onto the $\mathbf{q}$th Fourier component

$$\epsilon_{\text{eff}}^{-1}(\mathbf{q},\omega) = 1 + \frac{\rho^{\text{ind}}(\mathbf{q},\omega)}{\rho_0}. \tag{2.6}$$

If one assumes that the inhomogeneous medium has translational invariance at the macroscopic scale, an ensemble average of the effective inverse dielectric function of Eq. (2.6) can be made and Eq. (9) of Ref. 13 is obtained.

Instead, we consider a homogeneous isolated particle with local dielectric function ϵ_ω inside a box with local dielectric function ϵ_0, f being the relative part of the volume of this box occupied by the particle. The test charge density of Eq. (2.1) induces in the bulk of the particle and the host a charge with a single density Fourier component

$$\rho_b^{\text{ind}}(\mathbf{q},\omega) = \rho_0(\epsilon_\omega^{-1} - 1) \tag{2.7}$$

and

$$\rho_b^{\text{ind}}(\mathbf{q},\omega) = \rho_0(\epsilon_0^{-1} - 1), \tag{2.8}$$

respectively, and it also induces a surface charge density, which appears from the difference between the normal components of the electric fields created in and outside the surface

$$\sigma_s^{\text{ind}}(\mathbf{r},t) = \frac{1}{4\pi}[\boldsymbol{\nabla}\phi_s^{\text{ind}}(\mathbf{r},t)\cdot\hat{\mathbf{n}}|_{\mathbf{r}=\mathbf{r}^-} - \boldsymbol{\nabla}\phi_s^{\text{ind}}(\mathbf{r},t)\cdot\hat{\mathbf{n}}|_{\mathbf{r}=\mathbf{r}^+}], \tag{2.9}$$

where $\hat{\mathbf{n}}$ represents a unit vector in the direction perpendicular to the surface and $\phi_s^{\text{ind}}(\mathbf{r},t)$ is the scalar potential created by the induced surface charge. $\phi_s^{\text{ind}}(\mathbf{r},t)$ is determined by the continuity of the total scalar potential and the normal component of the displacement vector

$$\phi_s^{\text{tot}}(\mathbf{r},t)|_{\mathbf{r}=\mathbf{r}^-} = \phi_s^{\text{tot}}(\mathbf{r},t)|_{\mathbf{r}=\mathbf{r}^+} \tag{2.10}$$

and

$$\epsilon_0\boldsymbol{\nabla}\phi_s^{\text{tot}}(\mathbf{r},t)\cdot\hat{\mathbf{n}}|_{\mathbf{r}=\mathbf{r}^+} = \epsilon_\omega\boldsymbol{\nabla}\phi_s^{\text{tot}}(\mathbf{r},t)\cdot\hat{\mathbf{n}}|_{\mathbf{r}=\mathbf{r}^-}, \tag{2.11}$$

where ϕ^{tot} represents the total potential

$$\phi^{\text{tot}}(\mathbf{r},t) = \phi^{\text{ext}}(\mathbf{r},t) + \phi_b^{\text{ind}}(\mathbf{r},t) + \phi_s^{\text{ind}}(\mathbf{r},t), \tag{2.12}$$

with $\phi^{\text{ext}}(\mathbf{r},t)$ being the scalar potential created by the test charge and $\phi_b^{\text{ind}}(\mathbf{r},t)$ and $\phi_s^{\text{ind}}(\mathbf{r},t)$ being scalar potentials created by the charge induced in the bulk and the surface, respectively.

A. Spheres

The introduction of Eqs. (2.7)–(2.9) into Eq. (2.6) gives, for a spherical particle of radius a centered in a box of volume $\Omega \rightarrow \infty$,

$$\epsilon_{\text{eff}}^{-1}(\mathbf{q},\omega) = (1-f)\epsilon_0^{-1} + f\epsilon_\omega^{-1}$$
$$+ \frac{1}{4\pi\rho_0\Omega}\int d\mathbf{r}\, e^{-i(\mathbf{q}\cdot\mathbf{r} - \omega t)}\delta(r-a)$$
$$\times\left[\left.\frac{\partial\phi_s^{\text{ind}}(\mathbf{r},t)}{\partial r}\right|_{r=a^-} - \left.\frac{\partial\phi_s^{\text{ind}}(\mathbf{r},t)}{\partial r}\right|_{r=a^+}\right]. \tag{2.13}$$

Now, we introduce the well-known expansions, in terms of spherical harmonics, of a plane wave and also the Coulomb potential due to a point charge and find, after applying Eqs. (2.10) and (2.11):

$$\phi_s^{\text{ind}}(\mathbf{r},t) = \frac{(4\pi)^2\rho_0}{q}e^{-i\omega t}$$
$$\times\sum_{l=0}^{\infty}\sum_{m=-l}^{m=l}i^l Y_{lm}^*(\hat{\mathbf{q}})Y_{lm}(\hat{\mathbf{r}})G_l^s(\mathbf{q},\omega)f(r), \tag{2.14}$$

where

$$G_l^s(\mathbf{q},\omega) = \frac{\epsilon_\omega - \epsilon_0}{\epsilon_\omega l + \epsilon_0(l+1)}a^{l+2}$$
$$\times\left[-\epsilon_0^{-1}j_l'(qa) + (\epsilon_{\mathbf{q},\omega}^{-1} - \epsilon_0^{-1})j_{l+1}(qa)\frac{l+1}{2l+1}\right] \tag{2.15}$$

and

$$f(r) = \begin{cases} a^{-(2l+1)}r^l & \text{if } r \leq a \\ r^{-(l+1)} & \text{otherwise.} \end{cases} \tag{2.16}$$

Y_{lm} is the spherical harmonic function and j_l the spherical Bessel function of the first kind.

Then, the introduction of Eq. (2.14) into Eq. (2.13) gives the following result for the effective inverse longitudinal dielectric function of a homogeneous sphere of dielectric function ϵ_ω immersed in a medium of dielectric function ϵ_0:

$$\epsilon_{\text{eff}}^{-1}(\mathbf{q},\omega)=\epsilon_0^{-1}+f(\epsilon_\omega^{-1}-\epsilon_0^{-1})\Bigg\{1+3\sum_{l=0}^{\infty}(2l+1)$$

$$\times\Bigg[-\frac{\epsilon_0(l+1)}{\epsilon_\omega l+\epsilon_0(l+1)}\frac{j_l(qa)}{qa}j_{l+1}(qa)$$

$$+\frac{\epsilon_\omega l}{\epsilon_\omega l+\epsilon_0(l+1)}\frac{j_l(qa)}{qa}j_{l-1}(qa)\Bigg]\Bigg\},$$

$$(2.17)$$

and taking advantage of the identity[18]

$$\sum_{l=0}^{\infty}(2l+1)j_l(x)j_l'(x)=0, \qquad (2.18)$$

Eq. (2.17) can also be expressed as

$$\epsilon_{\text{eff}}^{-1}(\mathbf{q},\omega)=(1-f)\epsilon_0^{-1}+f\Bigg\{\epsilon_\omega^{-1}+3\sum_{l=1}^{\infty}l(2l+1)\Bigg[\frac{j_l(qa)}{qa}\Bigg]^2$$

$$\times\Bigg[-(l+1)/l\epsilon_0^{-1}-\epsilon_\omega^{-1}+\frac{(2l+1)^2/l}{\epsilon_\omega l+\epsilon_0(l+1)}\Bigg]\Bigg\}.$$

$$(2.19)$$

Equation (2.19) exactly coincides with the dilute limit $(f\to0)$ of the effective inverse dielectric function of Barrera and Fuchs[13] and the electron-energy-loss probability derived from this equation reproduces the results of Refs. 11 and 12.

If one assumes that the radius of the sphere is small, i.e., $qa\ll1$, an expansion of Eq. (2.17) with respect to qa gives, up to second order,

$$\epsilon_{\text{eff}}^{-1}(\mathbf{q},\omega)=\epsilon_0^{-1}+f(\epsilon_\omega^{-1}-\epsilon_0^{-1})\{1+f_{l=0}+f_{l=1}+f_{l=2}\},$$

$$(2.20)$$

where $f_{l=0}$, $f_{l=1}$, and $f_{l=2}$ represent monopole, dipole, and quadrupole contributions, respectively,

$$f_{l=0}=-1+\frac{4}{15}(qa)^2+O((qa)^4), \qquad (2.21)$$

$$f_{l=1}=-\frac{1}{5}(qa)^2+3\Bigg[1-\frac{1}{5}(qa)^2\Bigg]\frac{\epsilon_\omega}{\epsilon_\omega+2\epsilon_0}+O((qa)^4),$$

$$(2.22)$$

and

$$f_{l=2}=\frac{2}{3}(qa)^2\frac{\epsilon_\omega}{2\epsilon_\omega+3\epsilon_0}+O((qa)^4), \qquad (2.23)$$

and the introduction of Eqs. (2.21)–(2.23) into Eq. (2.20) gives

$$\epsilon_{\text{eff}}^{-1}(\mathbf{q},\omega)=\epsilon_0^{-1}+\epsilon_0^{-1}f\Bigg\{-3\frac{\epsilon_\omega-\epsilon_0}{\epsilon_\omega+2\epsilon_0}$$

$$+\Bigg[-\frac{1}{15}\frac{\epsilon_\omega-\epsilon_0}{\epsilon_\omega}+\frac{3}{5}\frac{\epsilon_\omega-\epsilon_0}{\epsilon_\omega+2\epsilon_0}-\frac{2}{3}\frac{\epsilon_\omega-\epsilon_0}{2\epsilon_\omega+3\epsilon_0}\Bigg]$$

$$\times(qa)^2+O((qa)^4)\Bigg\}. \qquad (2.24)$$

The first two terms of the right-hand side of Eq. (2.24) reproduce the well-known dilute limit of the Maxwell-Garnett dielectric function and the third term retains information about the structure of the medium through a dependence on the qa parameter.

B. Cylinders

For a homogeneous infinite cylinder of radius a and dielectric function ϵ_ω centered in a box of dielectric function ϵ_0 and volume $\Omega\to\infty$, the introduction of Eqs. (2.7)–(2.9) into Eq. (2.6) gives

$$\epsilon_{\text{eff}}^{-1}(\mathbf{q},\omega)=(1-f)\epsilon_0^{-1}+f\epsilon_\omega^{-1}$$

$$+\frac{1}{4\pi\rho_0\Omega}\int d\mathbf{r}\,e^{-i(\mathbf{q}\cdot\mathbf{r}-\omega t)}\delta(\rho-a)$$

$$\times\Bigg[\frac{\partial\phi_s^{\text{ind}}(\mathbf{r},t)}{\partial\rho}\Bigg|_{\rho=a^-}-\frac{\partial\phi_s^{\text{ind}}(\mathbf{r},t)}{\partial\rho}\Bigg|_{\rho=a^+}\Bigg],$$

$$(2.25)$$

where ρ represents the component of $\mathbf{r}$ in a plane perpendicular to the axis of the cylinder. Then, after the introduction of cylindrical Bessel functions and by requiring that the total scalar potential and the normal component of the displacement vector be continuous we find (see the Appendix) the expression for the scalar potential created by the induced charge at the surface of the cylinder

$$\phi_s^{\text{ind}}(\mathbf{r},t)=\frac{4\pi\rho_0}{Q^2+q_z^2}e^{i(q_z z-\omega t)}$$

$$\times\sum_{m=0}^{\infty}\mu_m i^m\cos(m\phi)G_m^s(\mathbf{q},\omega)f(\rho),$$

$$(2.26)$$

where

$$G_s(\mathbf{q},\omega)=(\epsilon_\omega-\epsilon_0)\frac{\epsilon_\omega^{-1}QJ_m'(Qa)+(\epsilon_\omega^{-1}q_z-\epsilon_0^{-1})I_m'(q_z a)f_m^{(1)}}{-\epsilon_\omega q_z I_m'(q_z a)+\epsilon_0 q_z I_m(q_z a)K_m^{-1}(q_z a)K_m'(q_z a)} \qquad (2.27)$$

and

$$f(\rho) = \begin{cases} I_m(q_z\rho) & \text{if } \rho \leqslant a \\ I_m(q_z a)K_m^{-1}(q_z a)K_m(q_z\rho) & \text{otherwise.} \end{cases}$$

(2.28)

Q and q_z represent components of the total momentum $\mathbf{q}$ in a plane perpendicular and in a direction parallel to the axis of the cylinder, respectively, J_m represents the cylindrical Bessel function of the first kind, I_m and K_m are modified Bessel functions, $f_m^{(1)}$ is given by Eq. (A10), and μ_m are Newmann numbers. Then we take advantage of the identities

$$q_z K_m'(q_z a)f_m^{(2)} = QJ_m'(Qa) - q_z I_m'(q_z a)f_m^{(1)}, \quad (2.29)$$

with $f_m^{(1)}$ and $f_m^{(2)}$ of Eqs. (A10) and (A11), and[18]

$$K_m^{-1}(x) = x[I_{m-1}(x) + I_m(x)K_m^{-1}(x)K_{m-1}(x)], \quad (2.30)$$

and the introduction of Eq. (2.26) into Eq. (2.25) gives

$$\epsilon_{\text{eff}}^{-1}(\mathbf{q},\omega) = \epsilon_0^{-1} + f(\epsilon_\omega^{-1} - \epsilon_0^{-1})\Bigg\{ 1 + \frac{2}{(Qa)^2 + (q_z a)^2}$$

$$\times \sum_{m=0}^{\infty} [\epsilon_\omega \alpha_m(q_z a) - \epsilon_0]^{-1} \frac{\mu_m J_m(Qa)}{K_m'(q_z a)I_m(q_z a)}$$

$$\times [\epsilon_\omega I_m'(q_z a)f_m^{(1)} + \epsilon_0 K_m'(q_z a)f_m^{(2)}] \Bigg\}, \quad (2.31)$$

where

$$\alpha_m(q_z a) = \frac{I_m'(q_z a)K_m(q_z a)}{I_m(q_z a)K_m'(q_z a)}. \quad (2.32)$$

The terms $\alpha_m(q_z a)$, which contain the surface plasmon modes, are in agreement with previous results for the energy-loss probabilities of electrons moving on definite trajectories,[3-6] and the energy-loss probability derived from Eq. (2.31) coincides with the integration over impact parameters of the energy loss of well-focused beams moving in a parallel direction to the axis of the cylinder.[19] In particular, if the momentum transfer is located in a plane perpendicular to the axis of the cylinder ($q_z a = 0$), Eq. (2.31) gives

$$\epsilon_{\text{eff}}^{-1}(\mathbf{q},\omega) = \epsilon_0^{-1} + f(\epsilon_\omega^{-1} - \epsilon_0^{-1})\Bigg\{ 1 - \frac{2}{Qa}J_0(Qa)J_1(Qa)$$

$$+ \frac{4}{Qa}\frac{1}{\epsilon_\omega + \epsilon_0}\sum_{m=1}^{\infty} J_m(Qa)$$

$$\times [\epsilon_\omega J_{m-1}(Qa) - \epsilon_0 J_{m+1}(Qa)] \Bigg\}. \quad (2.33)$$

III. ELECTRON ENERGY LOSS IN ZEOLITES

McComb and Howie[14] carried out valence-loss spectroscopy with four SiO_2 polymorphs of different density and determined, after a Kramers-Kronig analysis of the data, the real and imaginary parts of the dielectric function for each sample. The four SiO_2 polymorphs used were stishovite, co-

esite, α quartz, and silicalite. Stishovite is a high-density form of silica, with specific gravity of 4.28, and the other silica under study, coesite, α quartz, and silicalite, are less-dense polymorphs of specific gravity of 2.93, 2.66, and 1.79, respectively.[20] Their structure is built from SiO_4 tetrahedra with every silicon having four oxygens and every oxygen having two silicons as nearest neighbors.

McComb and Howie also determined, from the experimental spectra, the bulk-energy-loss functions $\text{Im}[-\epsilon_\omega^{-1}]$ for each silica polymorph investigated and found that the spectra from coesite, α quartz, and silicalite are all similar, showing an insensitivity of the plasmon peak to the density of the material, while the spectrum of the stishovite differs considerably. In Ref. 14 they regarded coesite, α quartz, and silicalite as less-dense versions of stishovite formed by mixing in some spherical spaces of vacuum in stishovite or stishovite in vacuum, but they were not able to interpret the experiments in terms of Maxwell-Garnett and other available versions of effective-medium theory. They also tried to regard coesite as the starting material to model α quartz and silicalite, but they were not able to reproduce the insensitivity of the position of the loss peak for these three materials.

On the other hand, it appears from the structure of these materials[20] that the modeling of zeolites by mixing spheres in an otherwise infinite medium is not appropriate. Instead, mixing in infinite cylinders in vacuum should model the structure of the zeolites under study more adequately and we have evaluated, therefore, from Eq. (2.31) the loss function $\text{Im}[-\epsilon_{\text{eff}}^{-1}(\mathbf{q},\omega)]$ of the zeolites under study.

The experiment shows a prominent peak in the loss function of stishovite, the most dense of the four materials, at $E = 31.2$ eV,[14] which can be identified with a bulk plasmon loss of plasmon frequency

$$\omega_p^2 = \frac{4\pi n e^2}{m_e} + \Omega^2, \quad (3.1)$$

n and $\hbar\Omega$ being the valence electron density and the band-gap energy, respectively. However, the peak in the loss function of the three other materials appears to be insensitive to the density of the material and could be identified instead with a surface plasmon loss. Therefore, we have taken stishovite as the reference material of dielectric function ϵ_ω and we have evaluated from Eq. (2.31) the loss function $\text{Im}[-\epsilon_{\text{eff}}^{-1}(\mathbf{q},\omega)]$ of coesite, α quartz, and silicalite, with filling fractions of 0.68, 0.62, and 0.42, respectively.

If one assumes that the radius of the cylinders is small $qa \leqslant 1$, the main features of the energy-loss function are controlled by the component of the momentum $\mathbf{q}$ in a plane perpendicular to the axis of the cylinder.[19] Consequently, we have taken $q_z a = 0$ and different values of Qa. The largest wave vector for which the bulk plasmon is a well-defined excitation is approximately equal to ω_p/v_F, v_F being the Fermi velocity; however, experimental valence-loss spectra were acquired by using an effective collection angle of 8.3 mrad, so that for a typical incident electron energy of 100 keV the largest transferred wave vector would be 5.89 Å^{-1} and this means that for cylinders with a radius of up to 5 Å the adimensional parameter Qa would take values of up to approximately 3.0.
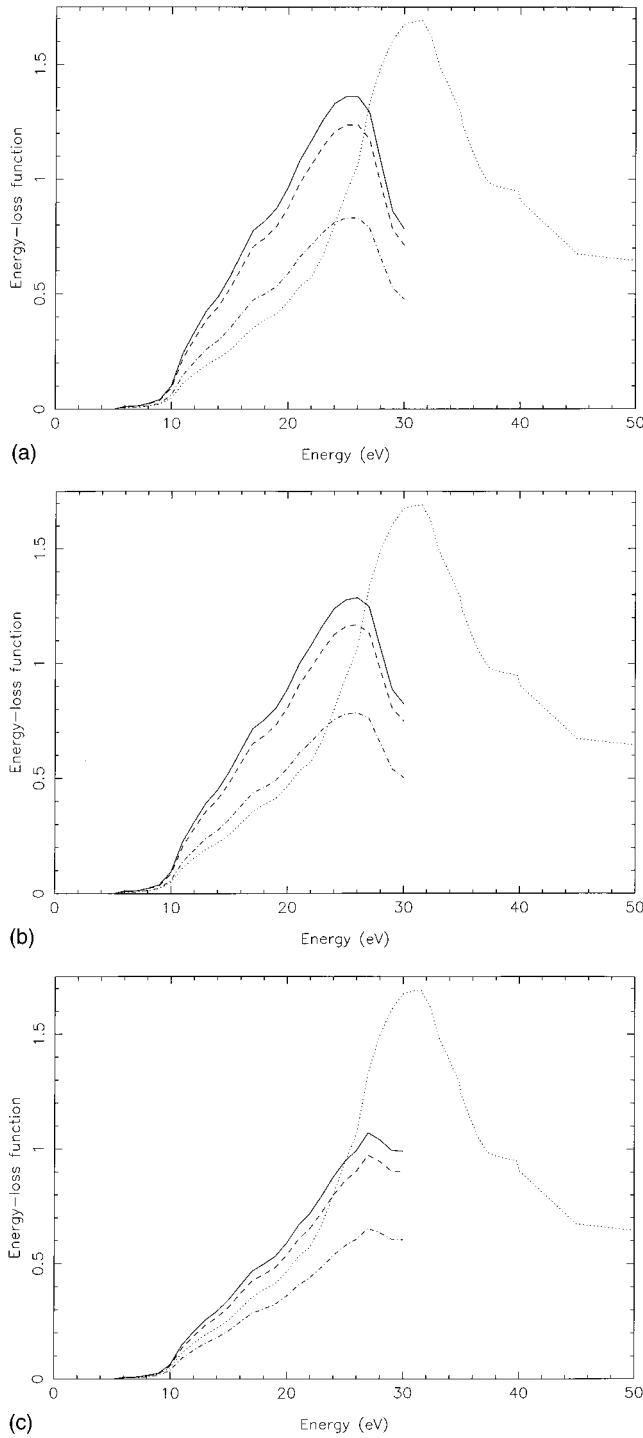
FIG. 1. Energy-loss functions $\mathrm{Im}[-\epsilon_{\mathrm{eff}}^{-1}(\mathbf{q},\omega)]$ for infinite cylinders of stishovite in vacuum with volume fractions $f = 0.68$ (solid line), 0.62 (dashed line), and 0.42 (dash-dotted line) to model coesite, α quartz, and silicalite, respectively, and three values of Qa: (a) 0.0, (b) 1.0, and (c) 3.0. Dotted lines represent the experimental loss function for stishovite.

The energy-loss functions $\mathrm{Im}[-\epsilon_{\mathrm{eff}}^{-1}(\mathbf{q},\omega)]$ calculated from Eq. (2.31) for coesite, α quartz, and silicalite on the basis of the experimental data for the dielectric function of stishovite are shown in Fig. 1, with three values of Qa: 0.0, 1.0, and 3.0. The bulk-energy-loss function of stishovite is also represented, showing a prominent peak for an electron
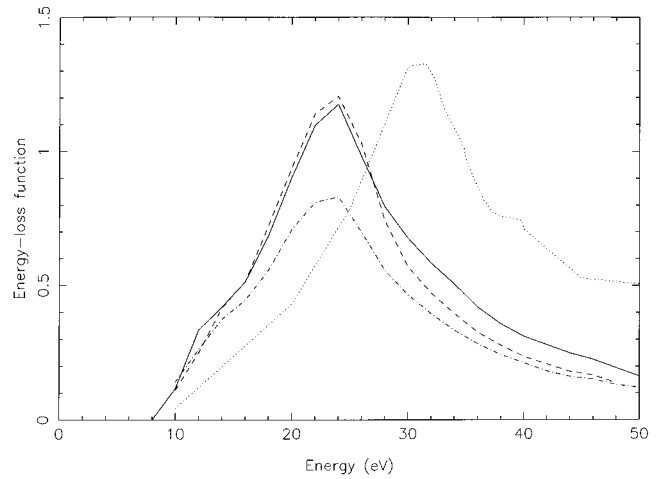

FIG. 2. Experimental loss functions for coesite (solid line), α quartz (dashed line), silicalite (dash-dotted line), and stishovite (dotted line), as taken from Ref. 14.

energy loss of 31.2 eV, which is identified with a bulk plasmon loss, as discussed above. Surface modes, described by the terms $\alpha_m(q_z a)$ of Eq. (2.32), are all very close to the planar mode[19] and, in particular, for $q_z a = 0$ they are all equal to the planar mode [see Eq. (2.33)]. Consequently, the peak near 24 eV in the loss function for coesite, α quartz, and silicalite is associated with surface modes. The height of these surface modes decreases as the parameter Qa increases as a consequence of the fact that the relative strength of the bulk mode increases with Qa, but it changes very little for values of Qa between 0 and 1. On the other hand, the effect of changing the volume fraction f to model different materials appears also in a variation of the surface mode height, the ratio between surface mode heights being equal to the ratio between the corresponding volume fractions.

The experimental loss functions are shown in Fig. 2.[14] It is obvious from Figs. 1 and 2 that peak positions are well described by our theory and also the insensitivity of the plasmon peak to the density of the material is explained. However, there are two discrepancies between our theory and the experiment. First, the ratio between the experimental surface mode heights is smaller than the ratio between volume fractions, which our theory predicts. Second, experimental surface modes exhibit a slight shift in position from 23.2 eV for the less-dense material, silicalite, to 24.0 eV for coesite. This is consistent with the expectations that for a collection of cylinders the plasmon peak should be sensitive to the filling fraction, appearing at larger energies as the filling fraction is increased and in the limit of $f = 1$ all losses being due to the bulk plasmon as the experimental data for stishovite indicates. This dependence on f cannot be explained within our theory, but within the range of densities for the three least-dense materials under study the position of the surface mode peak is expected to change very little, as shown by the experiment.

In the case of swift electrons moving with velocity $\mathbf{v}$ along the axis of the cylinders the probability per unit path length, per unit energy, for the electrons to transfer energy $\hbar\omega$ to the medium is[19]
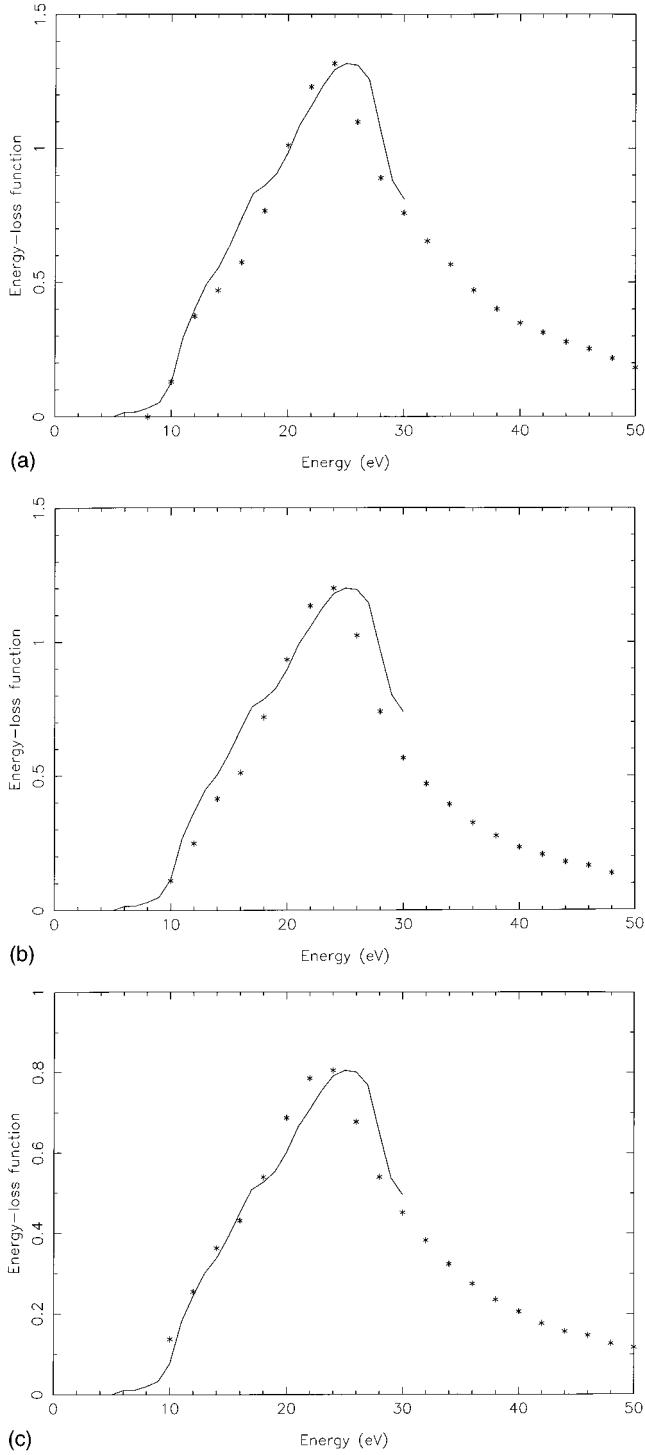
(a)

(b)

(c)

FIG. 3. Energy-loss function $F(\omega)$ as obtained from Eq. (3.2) with $v = 055c$ and $q_c a = 3.0$, for infinite cylinders of stishovite in vacuum with a volume fraction of (a) 0.68, (b) 0.62, and (c) 0.42 to model coesite, α quartz, and silicalite, respectively. The points indicated by an asterisk represent the corresponding experimental loss functions, as taken from Ref. 14.

$$P_\omega = \frac{2e^2}{\hbar^2 v^2} F(\omega), \qquad (3.2)$$
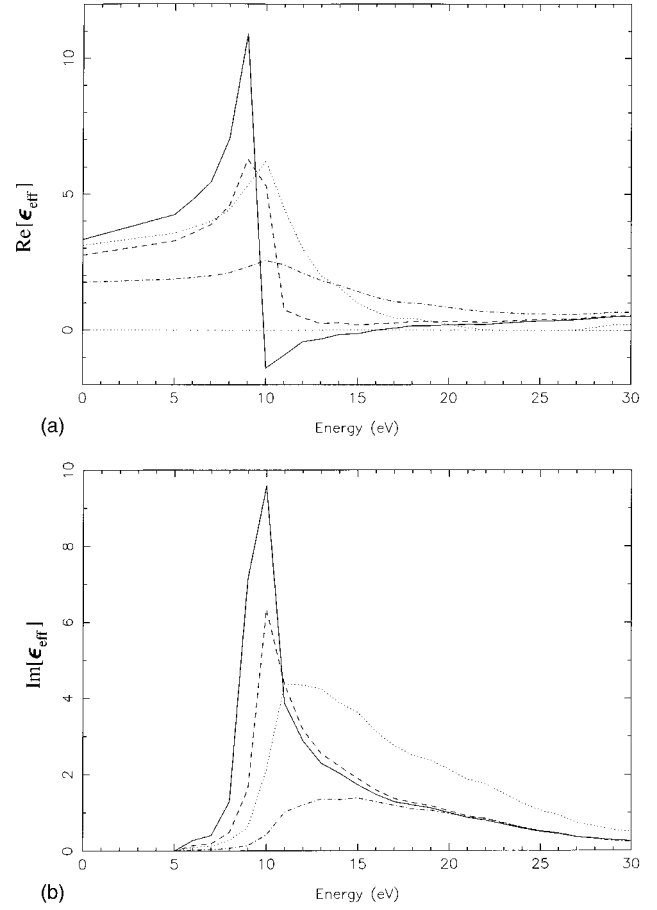
where

(a)

(b)

FIG. 4. Real and imaginary parts of the effective dielectric function of Eq. (2.31) with $Qa = 0.1$ and a volume fraction of 0.68, 0.62, and 0.42 to model coesite (solid line), α quartz (dashed line), and silicalite (dash-dotted line), respectively; the dotted lines represent the measured real and imaginary parts of the dielectric function of stishovite (Ref. 14). The real parts are represented in (a) and the corresponding imaginary parts in (b).

$$F(\omega) = \frac{1}{\pi} \int_0^{Q_c} dQ \frac{Q}{Q^2 + q_z^2} \mathrm{Im}[-\epsilon_{\mathrm{eff}}^{-1}(\mathbf{q}, \omega)], \qquad (3.3)$$

$\epsilon_{\mathrm{eff}}^{-1}(\mathbf{q}, \omega)$ being given by Eq. (2.31). Q_c represents the component of the largest transferred wave vector $\mathbf{q}_c$ in a plane perpendicular to the axis of the cylinder and

$$q_z = \frac{\omega}{v}. \qquad (3.4)$$

In Fig. 3 the experimental curves for the energy-loss functions for the materials under study are shown, together with our calculated results for the energy-loss function $F(\omega)$ of electrons traveling at $0.55c$, as obtained from Eq. (3.3) with $q_c a = 3.0$. It is clear that both peak positions and shapes are approximately well described by our theory. This agreement is also obvious (see Ref. 14) in Fig. 4, where the real and imaginary parts of our calculated effective dielectric functions are represented for $Qa = 0.1$.

IV. CONCLUSION

In conclusion, we have presented an alternative approach for the evaluation of the effective longitudinal response function of single isolated spheres and cylinders in an infinite medium. We have derived a general expression for the effective inverse dielectric function of isolated cylinders and we have applied our theory to explain valence-loss spectra from silica polymorphs of different density. We have explained the insensitivity of the plasmon peak with the density of the material by associating this peak with the existence of surface modes. Our theory for isolated cylinders predicts, of course, surface mode positions that are independent of the volume fraction f and we interpret the slight shift in position as the volume fraction increases as a consequence of the interaction between the cylinders, which has been neglected in our theory. The numerical approach to this problem recently developed[21] on the basis of photonic band-structure calculations[22] has been proved to be useful in the study of this interaction.[23] Work in this direction is now in progress.[24] A more detailed presentation of the derivation of the effective inverse longitudinal dielectric function of an isolated cylinder in an infinite medium will be presented elsewhere, in the frame of the self-energy formalism.[19]

APPENDIX: DERIVATION OF EQ. (2.26)

In order to study the response of an infinite cylinder we introduce the expansion of a plane wave[25]

$$e^{i\mathbf{Q}\cdot\boldsymbol{\rho}} = \sum_{m=0}^{\infty} \mu_m i^m J_m(Q\rho)\cos m\phi, \tag{A1}$$

where $\mathbf{Q}$ and $\boldsymbol{\rho}$ represent vectors located in a plane perpendicular to the axis of the cylinder, ϕ being the angle between them, J_m represents the cylindrical Bessel function of the first kind, and μ_m are Neumann numbers

$$\mu_m = \begin{cases} 1 & \text{for } m=0 \\ 2 & \text{for } m \geq 1. \end{cases} \tag{A2}$$

We also expand the Coulomb potential due to a positive unit point charge at $\mathbf{r}'$ as[26]

$$|\mathbf{r}-\mathbf{r}'|^{-1} = \frac{2}{\pi}\int_0^{\infty} dq_z \cos[q_z(z-z')]$$
$$\times \sum_{m=0}^{\infty} \mu_m I_m(q_z\rho_<)K_m(q_z\rho_>)\cos[m(\phi-\phi')], \tag{A3}$$

where $\rho_</\rho_>$ represent the smaller/larger of ρ and ρ', the components of $\mathbf{r}$ and $\mathbf{r}'$ in a plane perpendicular to the axis of the cylinder. z and z' represent the components of $\mathbf{r}$ and $\mathbf{r}'$ in the direction of the axis of the cylinder, $\phi-\phi'$ is the angle between ρ and ρ', and I_m and K_m are modified Bessel functions.

Now we replace, for simplicity, the dielectric function of the host ϵ_0 by 1 and consider the scalar potential created by the test charge density of Eq. (2.1),

$$\phi^{\text{ext}}(\mathbf{r},t) = \int d\mathbf{r} \frac{\rho^{\text{ext}}(\mathbf{r},t)}{|\mathbf{r}-\mathbf{r}'|}, \tag{A4}$$

and the potential created by the bulk charge density induced inside the cylinder,

$$\phi_b^{\text{ind}}(\mathbf{r},t) = \int_{\rho<a} d\mathbf{r} \frac{\rho_b^{\text{ind}}(\mathbf{r},t)}{|\mathbf{r}-\mathbf{r}'|}, \tag{A5}$$

where

$$\rho_b^{\text{ind}}(\mathbf{r},t) = \rho_0(\epsilon_\omega^{-1}-1)e^{i(\mathbf{q}\cdot\mathbf{r}-\omega t)}. \tag{A6}$$

Then the introduction of Eqs. (2.1) and (A6) into Eqs. (A4) and (A5) gives

$$\phi^{\text{ext}}(\mathbf{r},t) = \frac{4\pi\rho_0}{Q^2+q_z^2} e^{i(q_z z-\omega t)} \sum_{m=0}^{\infty} \mu_m i^m J_m(Q\rho)\cos m\phi \tag{A7}$$

and

$$\phi_b^{\text{ind}}(\mathbf{r},t) = \frac{4\pi\rho_0}{Q^2+q_z^2}(\epsilon_\omega^{-1}-1)e^{i(q_z z-\omega t)}$$
$$\times \sum_{m=0}^{\infty} \mu_m i^m G_m^b(\mathbf{q})\cos m\phi, \tag{A8}$$

where

$$G_m^b(\mathbf{q}) = \begin{cases} J_m(Q\rho)-I_m(q_z\rho)f_m^{(1)} & \text{if } \rho \leq a \\ K_m(q_z\rho)f_m^{(2)} & \text{otherwise,} \end{cases} \tag{A9}$$

with

$$f_m^{(1)} = q_z a J_m(Qa)K_{m-1}(q_z a) + Qa J_{m-1}(Qa)K_m(q_z a) \tag{A10}$$

and

$$f_m^{(2)} = q_z a J_m(Qa)I_{m-1}(q_z a) - Qa J_{m-1}(Qa)I_m(q_z a). \tag{A11}$$

Finally, we introduce Eqs. (A7) and (A8) into Eq. (2.12) and, after applying Eqs. (2.10) and (2.11), we find Eq. (2.26) with

$$G_m^s(\mathbf{q},\omega)$$

$$= (\epsilon_\omega-1)\frac{\epsilon_\omega^{-1}QJ_m'(Qa)+(\epsilon_\omega^{-1}-1)q_z I_m'(q_z a)f_m^{(1)}}{-\epsilon_\omega q_z I_m'(q_z a)+q_z I_m(q_z a)K_m^{-1}(q_z a)K_m'(q_z a)}, \tag{A12}$$

and if the cylinder is immersed in a medium of dielectric function ϵ_0, Eq. (A12) is easily found to be replaced by Eq. (2.27).

[1] P. M. Echenique and J. B. Pendry, J. Phys. C **8**, 2936 (1975).

[2] T. L. Ferrell and P. M. Echenique, Phys. Rev. Lett. **55**, 1526 (1985); T. L. Ferrell, R. J. Warmack, V. E. Anderson, and P. M. Echenique, Phys. Rev. B **35**, 7365 (1987).

[3] C. A. Walsh, Philos. Mag. **59**, 227 (1989).

[4] N. Zabala, A. Rivacoba, and P. M. Echenique, Surf. Sci. **209**, 465 (1989).

[5] A. Rivacoba, P. Apell, and N. Zabala, Nucl. Instrum. Methods Phys. Res. Sect. B **96**, 465 (1995).

[6] M. Schmeits, Phys. Rev. B **39**, 7567 (1989).

[7] M. Schmeits and L. Dambly, Phys. Rev. B **44**, 12 706 (1991).

[8] A. Rivacoba, N. Zabala, and P. M. Echenique, Phys. Rev. Lett. **69**, 3362 (1992).

[9] J. C. Maxwell-Garnett, Philos. Trans. R. Soc. London **203**, 385 (1904); **205**, 237 (1906).

[10] F. Fujimoto and K. Komaki, J. Phys. Soc. Jpn. **25**, 1769 (1968).

[11] D. R. Penn and P. Apell, J. Phys. C **16**, 5729 (1983). In Eq. (21) of this reference $\epsilon^{-1}(Q,\omega)$ should be replaced by $\epsilon^{-1}(Q,\omega)-1$, as pointed out by Barrera and Fuchs (Ref. 13).

[12] P. M. Echenique, J. Bausells, and A. Rivacoba, Phys. Rev. B **35**, 1521 (1987). The direct contribution to the screened interaction is missing in the first line of Eq. (5) of this reference. This contribution, together with part of the term represented in the second line of Eq. (5), would give the bulk contribution $\epsilon^{-1}-1$ to Eq. (7) of the same reference.

[13] R. G. Barrera and R. Fuchs, Phys. Rev. B **52**, 3256 (1995).

[14] D. W. McComb and A. Howie, Nucl. Instrum. Methods Phys. Res. Sect. B **96**, 569 (1995).

[15] L. A. Bursill, Pierre A. Stadelmann, J. L. Peng, and Steven Prawer, Phys. Rev. B **49**, 2882 (1994).

[16] Yu. E. Lozovik and A. V. Klyuchnik, in *Modern Problems in Condensed Matter Sciences*, edited by L. V. Keldysh, D. A. Kirzhnitz, and A. A. Maradudin (North-Holland, Amsterdam, 1989), Vol. 24.

[17] C. Kittel, *Quantum Theory of Solids* (Wiley, New York, 1963).

[18] *Handbook of Mathematical Functions*, edited by M. Abramowitz and I. A. Stegun (Dover, New York, 1965).

[19] J. M. Pitarke and A. Rivacoba, Surf. Sci. (to be published).

[20] W. A. Deer, R. A. Howie, and J. Zussman, *An Introduction to the Rock-Forming Minerals* (Longmans, London, 1966).

[21] J. B. Pendry and L. Martín-Moreno, Phys. Rev. B **50**, 5062 (1994).

[22] J. B. Pendry and A. MacKinnon, Phys. Rev. Lett. **69**, 2772 (1992).

[23] L. Martín Moreno and J. B. Pendry, Nucl. Instrum. Methods B **96**, 565 (1995).

[24] F. J. García Vidal, J. M. Pitarke, and J. B. Pendry (unpublished).

[25] F. Bowman, *Introduction to Bessel Functions* (Longmans, London, 1938), p. 90.

[26] J. D. Jackson, *Classical Electrodynamics*, 2nd ed. (Wiley, New York, 1965).